IOP Publishing Nanotechnology
Nanotechnology 27 (2016) 105702 (12pp) doi:10.1088/0957-4484/27/10/105702

Theoretical characterisation of point defects on a MoS_2 monolayer by scanning tunnelling microscopy

C González[1,2], B Biel[1] and Y J Dappe[2]

[1] Departamento de Electrónica y Tecnología de Computadores, Universidad de Granada, Campus de Fuente Nueva & CITIC, Campus de Aynadamar E-18071 Granada, Spain
[2] SPEC, CEA, CNRS, Université Paris-Saclay, CEA Saclay 91191 Gif-sur-Yvette Cedex, France

E-mail: cesar.gonzalez.pascual@gmail.es

Received 23 October 2015, revised 15 January 2016
Accepted for publication 19 January 2016
Published 10 February 2016

Abstract

Different S and Mo vacancies as well as their corresponding antisite defects in a free-standing MoS_2 monolayer are analysed by means of scanning tunnelling microscopy (STM) simulations. Our theoretical methodology, based on the Keldysh nonequilibrium Green function formalism within the density functional theory (DFT) approach, is applied to simulate STM images for different voltages and tip heights. Combining the geometrical and electronic effects, all features of the different STM images can be explained, providing a valuable guide for future experiments. Our results confirm previous reports on S atom imaging, but also reveal a strong dependence on the applied bias for vacancies and antisite defects that include extra S atoms. By contrast, when additional Mo atoms cover the S vacancies, the MoS_2 gap vanishes and a bias-independent bright protrusion is obtained in the STM image. Finally, we show that the inclusion of these point defects promotes the emergence of reactive dangling bonds that may act as efficient adsorption sites for external adsorbates.

Keywords: STM, DFT, 2D materials, MoS_2, defects

(Some figures may appear in colour only in the online journal)

1. Introduction

The possibility of isolating a single monolayer of graphene, as revealed in 2004 [1], has opened up a wide field of research in the study of bidimensional (2D) materials. Needless to say, graphene presents fantastic new electronic and mechanical properties that have been extensively studied [2–4], but other 2D materials with fascinating properties have emerged, such as hexagonal boron nitride (h-BN) [5], graphene oxide [6] and the large families of transition metal dichalcogenides (TMDC) [7–10]. Among them, MoS_2, which in its bulk form is a well-known dry lubricant and catalyser for low-sulfur diesel fuels in the industry [11], is a very promising material whose electronic properties are strongly thickness-dependent. Indeed, the MoS_2 bandgap evolves from being indirect in its bulk phase to become a larger direct bandgap when it is a monolayer [8]. This particular feature has provoked much interest in the realisation of MoS_2-based transistors [12], in particular in combination with graphene [13], where the former would provide the required gap for ON/OFF electronics, and the latter would provide fantastic electronic mobility. Its semiconductor character implies that MoS_2 is electronically passivated and thus many studies have considered its electronic and transport properties [14]. Moreover, theoretical calculations have recently suggested its chemical passivation because of its low reactivity with air [15]. However, this latter issue remains an open question and is still under debate.

However, it is commonly known in the context of nanoelectronic devices that the performance of this material is strongly dependent on its crystal quality. As such, defects like vacancies or substitutional atoms can have a huge influence on the reactivity and transport properties of MoS_2. Several studies have already been reported on this issue [16–18]. Noh *et al* studied S and Mo vacancies and their corresponding

interstitials in a MoS_2 monolayer theoretically using density functional theory (DFT). Zhou *et al* analysed different kinds of defects present in a MoS_2 monolayer by means of scanning transmission electron microscopy (STEM) experiments. They obtained atomic resolution and added further explanations via their own DFT simulations. Very recently, Hong and co-workers [18] extended defect analysis to substitutional atoms or antisites, again combining STEM measurements with new DFT calculations.

Although MoS_2 monolayers have been analysed intensively using various experimental and theoretical techniques, only a few recent works have presented systematic scanning tunnelling microscopy (STM) studies of this system that take the potential point defects into account [11, 19–22]. The very good resolution obtained in the STEM experiments has allowed us to understand the atomic arrangement of MoS_2 monolayers, but the electronic structure and, in particular, the semiconductor or metallic character, need to be determined by other techniques, such as STM. One of the first STM images of a monolayer MoS_2 was obtained by Sørensen *et al* [11]. The MoS_2 sheet was deposited over a gold substrate and a characteristic moiré pattern was found, similar to the one formed by graphene on different transition metals [23]. Inside the moiré, the brightest spots were associated with the sulfur atoms placed at higher positions. This assumption was recently corroborated [19]. In that work, the authors combined STM measurements with Tersoff–Hamann simulations in order to ascertain the impact of different vacancies and adatoms on the filled states image. However, the authors did not consider the substitutional cases, and their STM simulations were limited to S vacancies and one single negative bias voltage. In addition, the Tersoff–Hamman model has a well-known limitation because of the important role played by the *d*-electrons in some STM images, as has been previously shown [24].

Here, we present an exhaustive characterisation of Mo and S vacancies, as well as a great variety of antisite cases. Based on DFT calculations and STM image modelling, the evolution of MoS_2 passivation and metallicity is explored in the presence of point defects. Starting from the exact equation for the tunnelling current obtained within the Keldysh non-equilibrium Green function formalism, our calculations confirm that the sulfur atoms dominate in the STM images for a wide range of voltages in the pristine monolayer. On the other hand, the three vacancies analysed here (Mo, S and S divacancies) and the substitutional S atoms present different behaviours, depending on the applied voltage. We also find that the molybdenum atoms occupying the S sites induce a protrusion in the STM image (brighter than the one due to the S atoms in the defect-free monolayer), while the sulfurs are found to be hole depressions for most of the considered voltages.

The presence of such point defects in the single-layer crystal is well known for all the types of growing processes employed so far [17, 25]. The different defects must be carefully monitored, since they can dramatically alter the performance of future devices [26]. Our simulations thus provide a thorough theoretical characterisation of the STM images of a free-standing MoS_2 monolayer in the presence of S and Mo vacancies and antisites, taking into account full structural and electronic structure relaxation.

2. Method of calculation: MoS_2 model and STM calculation

A very efficient DFT localised-orbital molecular-dynamics technique (FIREBALL) was used for the structural relaxation of all the systems involved in this study. The computational scheme has been described in full detail elsewhere [27–29]. Hence, only the main points are summarised here. The code is based on a self-consistent version of the Harris–Foulkes local density approximation (LDA) functional [30, 31], where the standard Kohn–Sham (KS) potential is calculated by approximating the total charge with a superposition of spherical charges around each atom. The FIREBALL simulation package uses a localised, optimised minimal basis set [32], and the self-consistency is achieved over the occupation numbers through the Harris functional [30]. In addition, the LDA exchange–correlation energy is calculated using the efficient multi-centre weighted exchange–correlation density approximation (McWEDA) [28].

Firstly, the perfect MoS_2 crystalline structure is simulated using the FIREBALL–DFT code as a reference point for the subsequent study of substitutional defects and vacancies. Using a simple basis set of orbitals with cutoff radii (in atomic units) [29] of $s = 3.1$ and 6.2, and $p = 3.9$ and 6.2 for S and Mo, respectively, and $d = 5.8$ (for Mo), the obtained lattice constant for the perfect unit cell is 3.185 Å, in good agreement with the experimental evidence [33]. In figure 1(a), the frontal view (upper part of the figure) shows a 6×4 rectangular unit cell of MoS_2 with the atomic arrangement mixing the Mo and the S atoms in a hexagonal pattern. In the lower part of the figure, the lateral view shows the sulfurs at an equilibrium distance of 1.51 Å above and below the Mo atoms. The convergence of the system is achieved using a set of 64 *k*-points in the Brillouin zone until the forces reach a value lower than 0.05 eV/Å.

In a second step, the most relevant vacancies and antisite defects were recreated in the 6×4 rectangular unit cell in order to determine their influence on the structural and electronic properties using the same conditions mentioned previously. This unit cell was tested to ensure that it was large enough to avoid interaction between defects in neighbouring supercells (similar to [19]). In all the calculations, an isolated monolayer of MoS_2 was considered, without substrate underneath. This would be electronically equivalent to a situation where the MoS_2 monolayer was deposited onto a non-reactive substrate, like a chemically and electronically passivated semiconductor. The effect of this kind of substrate on the electronic structure of the MoS_2 was predicted to be negligible, as demonstrated by calculations for MoS_2 on SiO_2 [34] and experimental measurements [35]. A substrate of this kind is highly desirable in order to reduce the interaction of defects with a reactive surface.

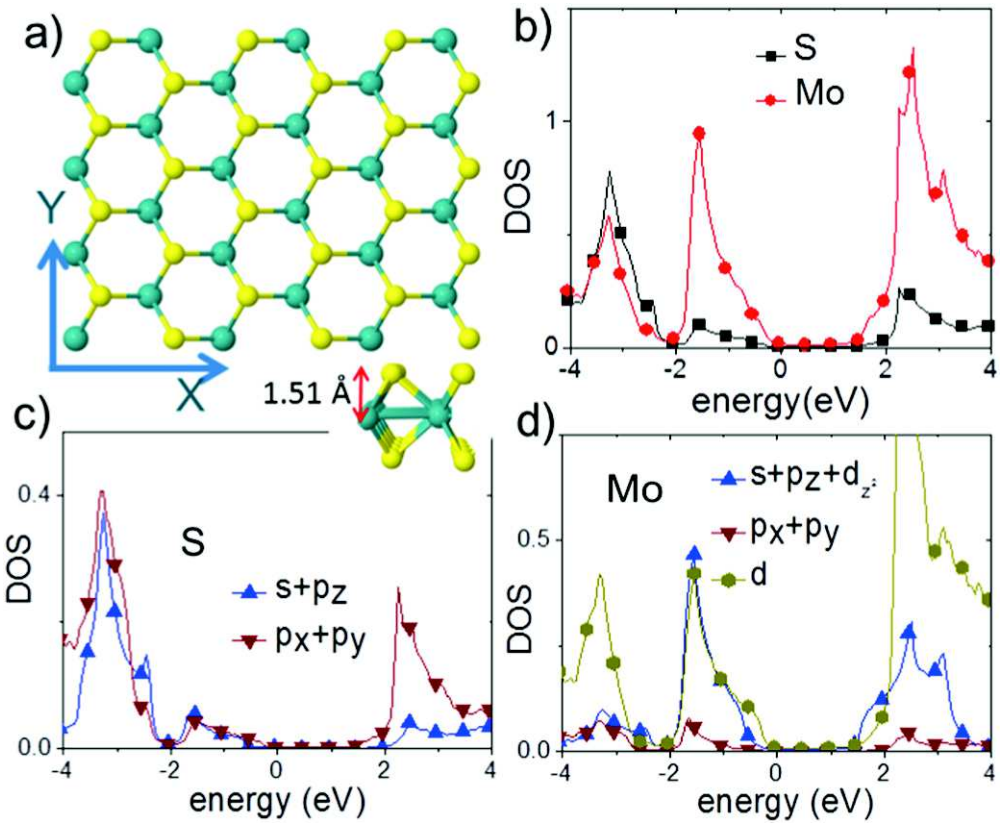

Figure 1. (a) Top and side view of the atomic structure of a clean single layer of MoS_2 (yellow/blue spheres are S/Mo). The arrows indicate the *X* and *Y* directions of the lattice vectors used in the calculation. (b) Calculated electronic DOS for S (black squares) and Mo (red circles) atoms; (c) and (d) show the orbital contributions to the atomic DOS of the S and Mo atoms, respectively. The DOS are separated into directional $s + p_z + d_{z^2}$ orbitals (blue up-triangles), in-plane $p_x + p_y$ orbitals (red down-triangles) and the sum of the other four *d* orbitals (yellow hexagons).

Once the equilibrium geometry is obtained, the contribution of the two atomic species to the density of states (DOS) is calculated. Figure 1(b) represents the DOS of the Mo and S atoms in the perfect MoS_2 monolayer. An electronic gap of around 1.7 eV is found, in good agreement with the optical gap measured experimentally [8, 36, 37] and other theoretical LDA-based calculations [34]. The Mo contribution (red curve) dominates the electronic density at both sides of the gap, as previously reported by DFT calculations [18, 19]. Figures 1(c) and (d) show the orbital contributions of the S and Mo atoms, respectively. We have separated the DOS into three (two) different contributions for the Mo (S) atom: firstly, the directional $s + p_z + d_{z^2}$ orbitals (blue up-triangles), secondly, the in-plane $p_x + p_y$ orbitals (red down-triangles) and finally, the sum of the other four *d* orbitals (yellow hexagons). The implications of these features for the STM images are discussed below.

In order to obtain a visual description of the influence of the defects, we also performed STM calculations to compare with the experimental results. The theoretical simulations of the STM current were based on the nonequilibrium Green function technique developed by Keldysh [38]. Within this methodology, the complete system can be divided into two isolated subsystems: the tip (T) and the sample (S), coupled by a weak tip–sample interaction ($T_{TS/ST}$). These subsystems are treated separately and are finally joined in the equation of the electronic current for an applied voltage *V* at 0 K temperature:

$$I = \frac{4\pi e^2}{h}\int_{E_F}^{E_F+eV} \mathrm{Tr}[T_{TS}\rho_{SS}(\omega)D^r_{SS}(\omega) \times T_{ST}\rho_{TT}(\omega - eV)D^a_{TT}(\omega - eV)]d\omega, \quad (1)$$

where ρ_{TT} and ρ_{SS} are the density matrices associated with the subsystems tip and sample, respectively, and the D^a_{TT} and D^r_{SS} matrices are related to the multiple scattering effect produced by the electronic reflections that might take place when the tip is close to the sample. For normal tunnelling distances (between 5 and 7 Å), these matrices tend to the identity, thus simplifying the final equation. All the required quantities for these calculations are extracted directly from the FIREBALL Hamiltonian after geometrical optimisation, as described above. A complete description of the methodology can be found in [39, 40].

The metallic tip considered for the calculations is a four-layer Au(111) slab with 5×5 periodicity, coupled to a pyramid cluster of four gold atoms terminated by a single apex, which has previously been used successfully on molecules [41] and graphene [42]. The tip is fully relaxed with FIREBALL, using 16 *k*-points in the first Brillouin zone, with

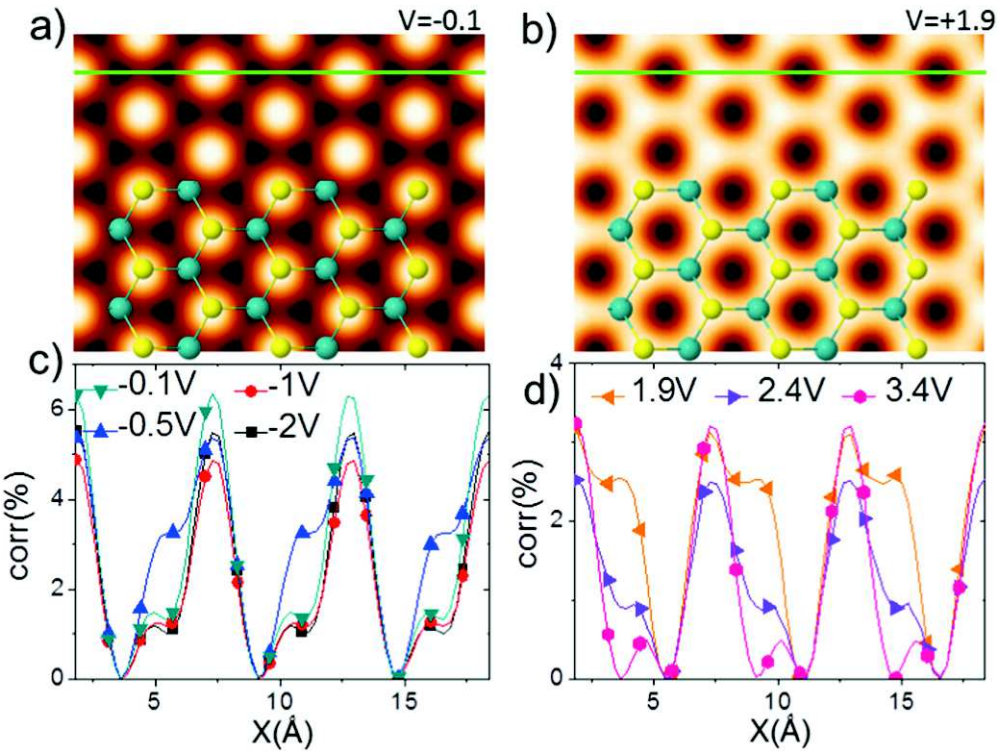

Figure 2. Calculated STM images at 4.5 Å and a bias of (a) −0.1 V and (b) +1.9 V for a clean MoS_2 monolayer. The STM images were graphed using WSxM software [44]. The green line indicates the selected direction for (c) and (d), where the cross-sectional profiles are shown for the different filled and empty state voltages studied in this work, respectively. The corrugation is represented by the percentage change obtained in the current at the different points with respect to the lowest value.

the same force tolerance set for the MoS_2 monolayer. Once the relaxed structure is obtained, the DOS can be calculated.

Finally, the $T_{TS/ST}$ terms are estimated using the dimer approximation: a dimer of each couple of elements is created for different distances and the value is subsequently interpolated during the STM calculation. A more detailed explanation of the DFT-based STM methodology can be found in [40].

In the following sections, we compare the DOS and STM images obtained for the different vacancies and substitutional atoms in MoS_2 to the perfect MoS_2 crystal. Our purpose is to determine the influence of such defects on the electronic properties and STM images of the material. The images were calculated in a constant height mode for several tip–sample distances (4.0 Å, 4.5 Å and 5.0 Å) and for a range of voltages, accounting for both the filled and empty states, namely 0.1, 0.5, 1.0, 1.5 and 1.9 V. While in some cases a substantial change with the applied voltage was found in the STM image, the defect images showed no alteration with the tip height. The images presented in this paper were calculated at 4.5 Å. At these distances, multiple scattering effects can be ignored, thus simplifying the calculation.

3. STM images of the ideal MoS_2 monolayer

In the previous section, the atomic configuration and DOS of the MoS_2 monolayer were presented in figure 1. We will now proceed to relate the simulated STM images displayed in figure 2 to the electronic and structural properties of the MoS_2 monolayer.

Looking at the DOS presented in figure 1(b), the Mo atoms would be expected to appear brighter in the STM simulations due to their higher contribution to the DOS compared to the S atoms. However, our simulated STM image for the filled states (figure 2(a)) shows the opposite, with S atoms appearing as a protrusion and Mo atoms appearing as depressions in a triangular pattern. In figures 1(c) and (d) the DOS is decomposed into two or three different contributions for S and Mo atoms, respectively: the directional $s + p_z + d_{z^2}$ orbitals, the in-plane $p_x + p_y$ orbitals and the sum of the other four d orbitals. The contributions from the directional and non-directional orbitals are similar in both kinds of atoms and, consequently, the current will be dominated by the $s + p_z + d_{z^2}$ orbitals. This orbital decomposition clearly shows that the Mo atoms still present a much higher contribution from the directional orbitals in the DOS. However, the S atoms appear much brighter in the STM image, meaning that the geometrical effects dominate in this system. This assumption can be explained in terms of the tip–sample coupling. The probability of an electron hopping from the tip to the sample decays exponentially with the distance, which strongly influences the value of the current due to the quadratic dependence of matrices $T_{TS/ST}$ on equation (1). As discussed earlier, the S atoms are located 1.51 Å higher than the Mo atoms and, consequently, the tip–Mo hopping will be much lower than for the tip–S case, which compensates the higher Mo contribution to the DOS.

Even though the image in figure 2(a) is calculated for a voltage of $V = -0.1$ V, similar images were obtained for higher voltages. Our result thus corroborates previous findings by other authors [11, 19]. For instance, Altibelli *et al* found a contrast change in their simulated STM image of a MoS_2 surface: for close tip–MoS_2 distances, the Mo atoms were observed as a bright protrusion [43]. Using the methodology presented here, this result can be found for small distances when the multiple scattering effects are included in the calculation. For such small distances, the current saturates over the S atoms while the tip–Mo interaction increases, producing current growth over the Mo atoms. As a result, the contrast change can be obtained. Nevertheless, this feature only appears in the contact regime, where other important effects such as atomic and charge rearrangement should also be taken into account.

By contrast, for positive voltages the Mo atoms can be imaged along with the S atoms, as shown in figure 2(b). From $V = +1.5$ V to $V = +1.9$ V (see the total DOS and the orbital contributions shown in figures 1(b) and (c) as a reference), the DOS of the S atoms is very small, while the Mo contribution grows very quickly. As a result, the electronic distribution practically compensates the height effect and, consequently, the final image displays an asymmetric hexagonal pattern. For higher voltages, the DOS of the S atoms grows enough to finally recover a triangular pattern similar to the one obtained for the filled states. This argument can also explain the larger gap of 2.4 eV measured very recently by Huang *et al* when using the scanning tunnelling spectroscopy (STS) technique on a MoS_2 monolayer deposited over a graphite substrate [37]. As the tunnelling current is dominated by the S atoms and their contribution to the DOS is very low for energies up to +2 eV, the current change is very small when the bias is increased. Consequently, the derivative dI/dV in the STS experiment could be small enough to produce a larger gap than the optical one found in the same work using the photoluminescence technique, as well as the gap deduced from our calculated DOS.

In figures 2(c) and (d) the cross-sectional profiles are represented. Each line shows the current change along the direction indicated by the green line in the STM maps for the different biases studied in this work. In order to have a direct comparison for all the different voltages, we considered the percentage change in the current, defined by $(I - I_{min})/I_{min}$, as done previously by Altibelli *et al* [43]. In that work, calculations were performed for a MoS_2 crystal instead of a single layer, and for this reason, some electronic changes can be expected. Thus, for a tip–sample distance of 4.5 Å and a negative bias, we obtained a corrugation of around 6 %, while a larger value was obtained in the perfect crystal (25 %). Note that our corrugation was quite stable for all the negative voltages applied to the monolayer, only varying from 5 to 6.2 %. The corrugation on the empty state voltages again remained quite constant, but in a slightly lower range (between 2.5 and 3.3 %). Comparing the filled and empty states curves, a small change can be inferred in the high voltage images, i.e., ±2 V. The difference is almost imperceptible in the resulting STM image, as shown, for example, for the −0.1 V case (figure 2(a)), where the Mo atoms and hollow sites are almost indistinguishable.

4. Unravelling the STM images of the defective systems

4.1. Molybdenum single vacancy

We turn now to the case of the molybdenum vacancy, which is created when a single Mo atom is removed from the ideal MoS_2 monolayer. Figure 3(a) shows the overall geometry of the cell once a Mo atom has been removed. The general structure has not been greatly affected, since the second neighbour distance is too large in MoS_2 to allow the creation of new bonds and hence further reconstruction. Therefore, none of the atoms is displaced by more than 0.1 Å from their original positions, and the neighbouring S and Mo atoms around the vacancy will consequently present dangling bonds. This is reflected in the strong modifications to the electronic DOS of the system (figure 3(b)), where localised states associated with the unsaturated bonds of both Mo and S neighbouring atoms now show up in the midgap. These new peaks were obtained by different groups in previous DFT calculations [16, 19]. In order to determine their origin, the orbital decomposition performed in the pristine monolayer is done here for the S and Mo atoms close to the vacancy, as shown in figures 3(c) and (d), respectively. The $p_x + p_y$ character of the sulfur peaks confirms the relationship with the unsaturated bonds. As a consequence, the overall gap decreases by almost 1 eV, which corresponds to the creation of the dangling bonds. The effect on the gap size of the point defects studied in this work is summarized in table 1.

The details discussed above have an important impact on the calculated STM image shown in figure 3(a). In this case, a positive bias of +1.9 V was used to take into account the new peaks found in the originally pristine gap. The image thus shows three brilliant traces located in the neighbouring hexagons around the vacancy. None of these features falls over the S atom closest to the vacancy. This fact stresses the *p*-character of the S dangling bond, oriented in the opposite direction to the original bond. This assumption is further confirmed by the images calculated for −1.9 V (not shown here), where the effect of the dangling bond is reduced and three spots are relocated over the S atoms. It is important to note that the three S atoms are imaged more brightly in this defective crystal than in the perfect monolayer for all the applied voltages, which proves the strong influence of the Mo vacancy on the charge redistribution. Therefore, as expected, a higher reactivity for this site can be deduced from the reduction of the gap and the brighter appearance of the dangling bonds in the STM image. As a consequence, this defect may be very useful for facilitating, for instance, molecular adsorption for 2D nanosensors.

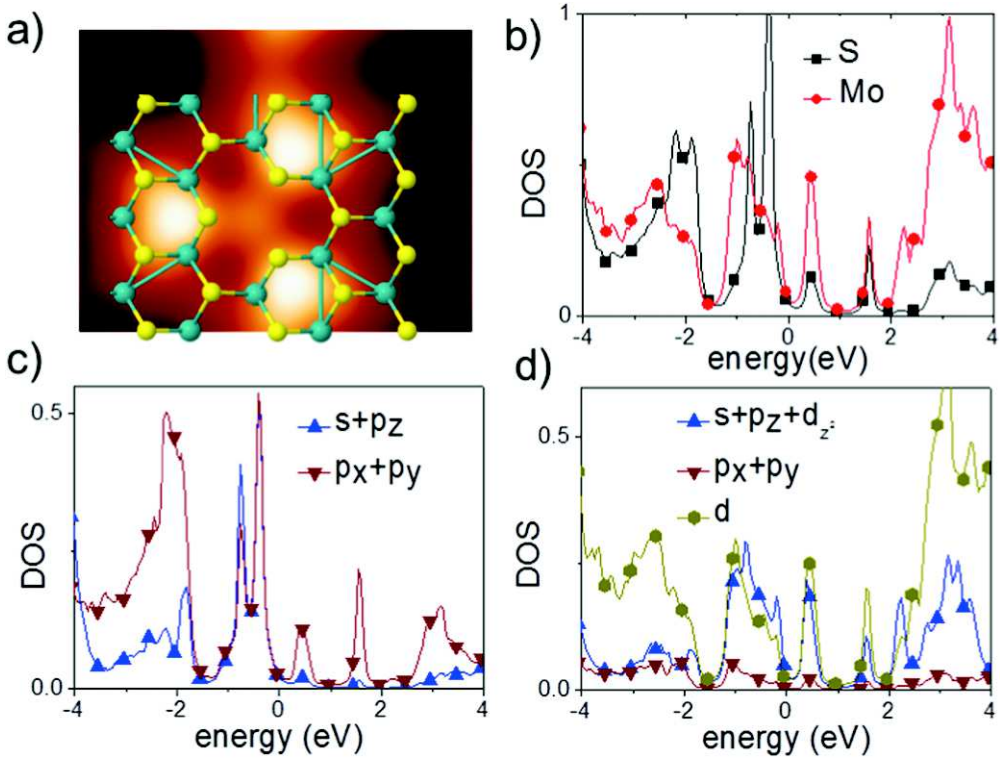

Figure 3. (a) STM image of the unoccupied states ($V = +1.9$ V) with the atomic configuration superimposed (yellow/blue spheres represent S/Mo atoms) for a Mo vacancy. The corresponding electronic DOS are represented in (b) for one S (black squares) and one Mo (red circles) atom close to the vacancy, while (c) and (d) show the orbital contributions to the atomic DOS of the S and Mo atoms close to the vacancy, respectively. The DOS are separated into directional $s + p_z + d_{z^2}$ orbitals (blue up-triangles), in-plane $p_x + p_y$ orbitals (red down-triangles) and the sum of the other four d orbitals (yellow hexagons).

Table 1. Energy gap (E_g in eV for the different structures analysed in this work: clean MoS_2, Mo/S vacancy (V-Mo/S), Mo vacancy with one S (V-Mo+S) or two S (V-Mo+S2) atoms (and the opposite case, changing S and Mo in the vacancy) and a S divacancy (V-S2) with one (V-S2+Mo) or two Mo (V-S2+Mo2) atoms. *In this structure, there is a gap of 1.25 eV on the empty states side after the half-occupied state at the Fermi level.

	Clean	V-Mo	V-Mo+S	V-Mo+S2	V-S	V-S+Mo	V-S2	V-S2+Mo	V-S2+Mo2
E_g(eV)	1.70	0.64	0.60	1.25*	1.0	no gap	0.80	no gap	no gap

4.2. Molybdenum antisite: one substitutional S atom

In a second step, the missing Mo atom is substituted by an extra S atom. Starting from the geometry with the S atom occupying exactly the original Mo site, the structure is relaxed following the same conditions used in the previous cases. Then, the substitutional S atom moves from its initial position, trying to find the environment that will optimise the bonding with two Mo and four S atoms. As a result, an asymmetric configuration with respect to the previous one is obtained. It is important to note that the substitutional atom remains in the same plane as the Mo atoms. This final structure is superimposed on the STM image of figure 4(a). Regarding the electronic properties, figure 4(b) shows the DOS of the substitutional S (labelled S-sub) and one Mo bonded to this substitutional atom (labelled Mo-b), while figure 4(d) shows the S atoms close to the original Mo vacancy, labelled S-1 (close to the substitutional atom) and S-2 (far away). As a first remark, we can observe a very sharp and intense peak of the S-sub atom at around 1.5 eV above the Fermi level. This S atom is only partially bonded to two Mo atoms. Hence the peak corresponds to a localised unoccupied state with a strong p-character, mostly due to the p_z orbital. In addition, the top conduction band of the Mo-b atom has been moved backwards to its initial energy position in the ideal crystal below the Fermi level. The shift is due to the new hybridisation with the S-sub atom. Finally, the peak in the gap due to S-2 atoms appears at +0.5 eV, while stronger unoccupied states can be observed between 1 and 2 eV due to the S-1 atom.

In order to take into account all these new features, the STM image showcased in figure 4(a) was again calculated for a bias of +1.9 V. Comparing this with the Mo vacancy case, we can observe one spot with reduced brightness, whereas the two other spots appear larger, close to the substitutional atom. Although the new sulfur makes a large contribution to the DOS, its lower height implies a lower contribution to the current. On the other hand, if the voltage is reduced to

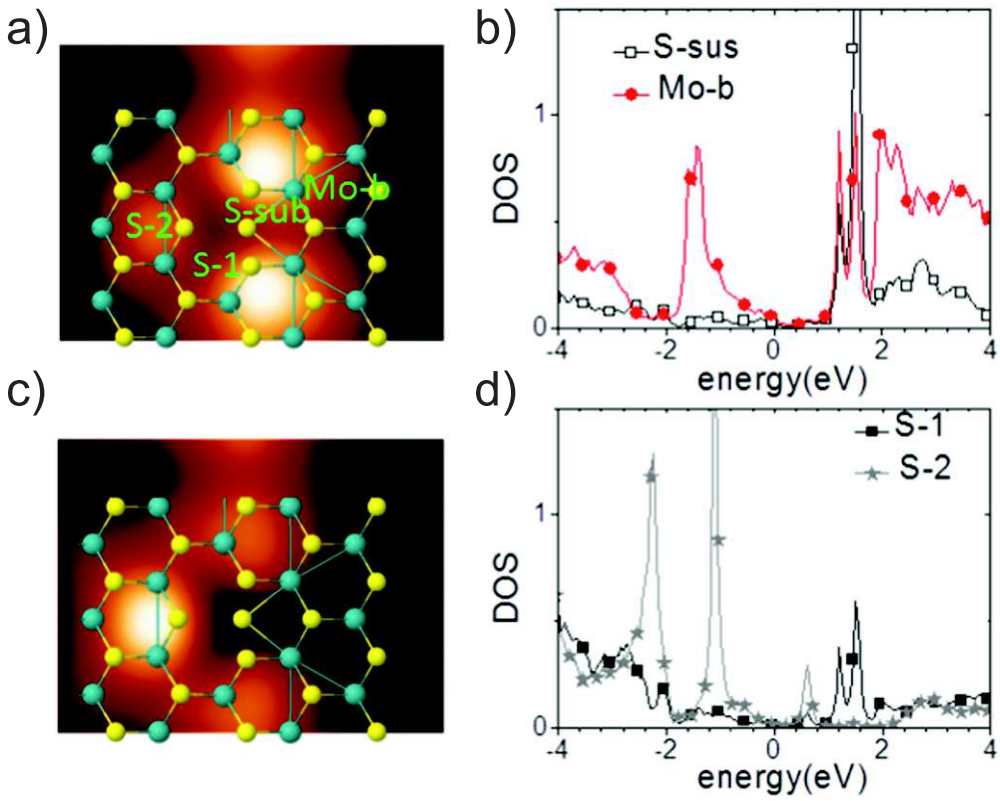

Figure 4. (a) STM image of the empty states ($V = +1.9$ V) with the atomic configuration superimposed (yellow/blue spheres represent S/Mo atoms) for a Mo vacancy with a substitutional S atom. The corresponding electronic DOS are represented in (b) for the S atom (open black square) occupying the Mo vacancy (S-sub) and a Mo atom (red circles) bonded with a S-sub (Mo-b). The STM image calculated at +0.5 V is shown in (c) and in (d) the DOS of two different S atoms around the vacancy, labelled S-1 (black squares) and S-2 (grey stars), is presented.

+0.5 V, the contrast is modified (see figure 4(c)), leading to a bright spot on the S-2 atom due to the aforementioned peak. Interestingly, in the occupied states the resulting image looks similar to the empty states one, due to the strong peak located at −1.0 V in the DOS associated with the same S-2 atom. Consequently, the inclusion of a S atom in the Mo vacancy leads to an asymmetric image that depends strongly on the applied voltage.

4.3. Molybdenum antisite: two substitutional S atoms

Starting from the previous configuration, a second S atom can be added to the Mo vacancy. Intuitively, the S atoms would try to mimic their standard S positions in the perfect monolayer, but now on the Mo site. The resulting relaxed structure confirms this assumption and both S atoms are placed on the same *XY* position 3.0 Å one above the other. Consequently, as shown in figure 5(a), where the optimised geometry is superimposed on the STM image, only one substitutional S atom is visible. Now the relaxed structure looks like a standard MoS_2 monolayer, but its corresponding STM image shows striking differences with respect to the one for the pristine crystal. It is worth mentioning that these two substitutional atoms are no longer connected to Mo atoms, but rather to the neighbouring S atoms. For symmetry considerations, the additional S atoms are now located on the vacancy, but the unit cell is still appreciably deformed, increasing the size of the vacancy site. As a consequence of the newly established S–S bonds, two pronounced peaks appear in the DOS within the MoS_2 gap (figure 5(b)), leading to an increased metallicity of the MoS_2 layer. The first peak at the Fermi level has a $s + p_z$ component as shown in figure 5(d), while the second one has an in-plane $p_x + p_y$ character. This implies that the S-sub atoms remain in a semi-occupied state, thus producing a fourth spot over the substitutional atoms for low voltages (see figure 5(c)). As in the previous case, the image changes when the voltage is increased, as shown in figure 5(a). Now the original image of the pristine MoS_2 is recovered, but with a dark hole over the vacancy site due to the lower height of the substitutional sulfur compared to the standard S atoms.

Note that in this case the atomic rearrangement leads to the formation of a new gap of 1.25 eV, starting from the half-occupied state at the Fermi level, as shown in table 1. Thus, defects are an interesting way of tuning the electronic structure of the sample in a given energy range.

From the results obtained for the three cases containing a Mo vacancy in the otherwise pristine MoS_2 monolayer, we can conclude that the absence of one Mo atom leads to a potentially reactive site that will enhance molecular or atomic adsorption. This could be exploited for electronic applications, since the neighbouring dangling bonds can be located

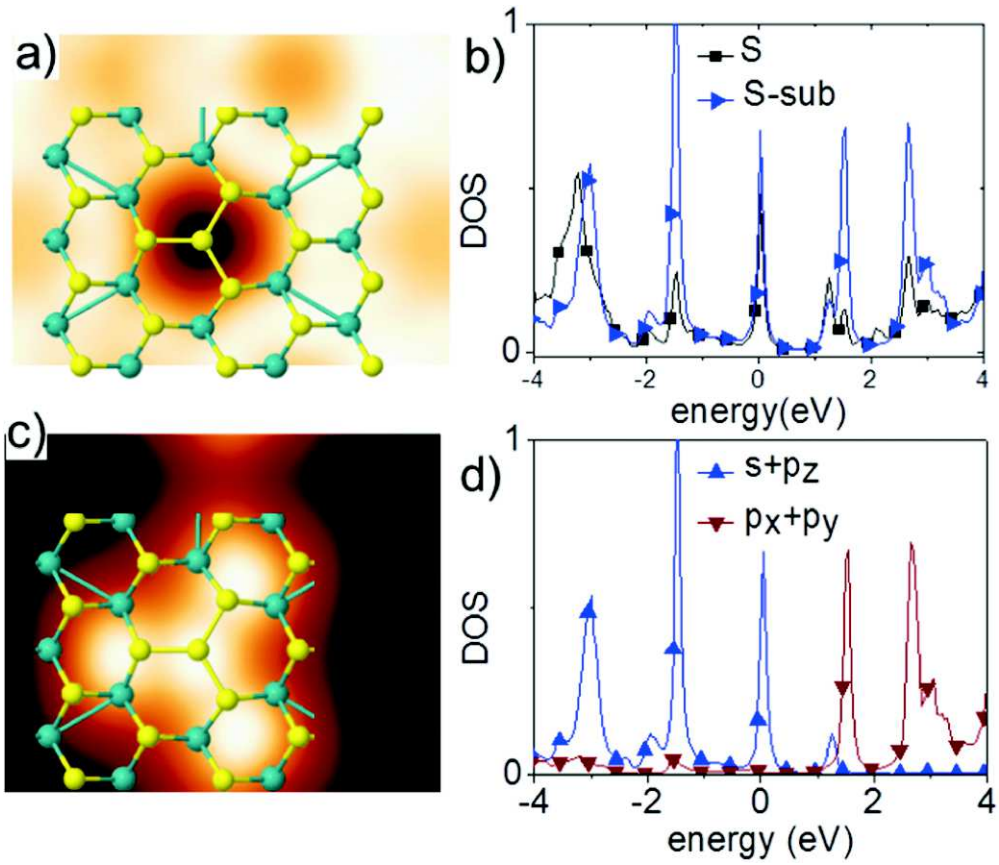

Figure 5. (a) STM image of the unoccupied states ($V = +1.9$ V) with the atomic configuration superimposed (yellow/blue spheres represent S/Mo atoms) for a Mo vacancy with two substitutional S atoms (the second S atom is 3.0 Å below the one presented in the structure). The corresponding electronic DOS are presented in (b) for one S atom (blue triangle) occupying the Mo vacancy (S-sub) and another S (black squares) bonded with it. The STM image calculated at +0.5 V is shown in (c) and (d) shows the orbital contributions to the atomic DOS of the substitutional S atoms: directional $s + p_z$ orbitals (blue up-triangles) and in-plane $p_x + p_y$ orbitals (red down-triangles).

easily in the STM images. However, when the Mo atom is replaced by one or two S atoms, these dangling bonds progressively vanish, leading to a partially occupied state at the Fermi level and increasing the MoS_2 metallicity. In this manner, a Mo vacancy combined with one or two S substitutional atoms represents an interesting way to tune the reactivity of a MoS_2 adsorption site.

4.4. Sulfur single vacancy

We now turn to the S vacancy, removing one S atom from the original pristine MoS_2 monolayer. The resulting relaxed structure is superimposed on the STM image in figure 6(a). The first consequence is a small contraction (less than 0.05 Å) of the Mo network around the S vacancy, due to the lower electronic density. In the DOS displayed in figure 6(b) an important reduction of the Mo gap (around 0.7 eV) with respect to the ideal structure is found (see the value in table 1). Additionally, and due to the absence of the S atom, the unbounded Mo orbitals trigger the emergence of a very intense and sharp peak at 1 eV above the Fermi level. The DOS of this atom is decomposed in figure 6(d), showing a complete *d*-character (even the directional contribution is due to the d_{z^2} orbital). This is reflected in the STM image shown in figure 6(c) and simulated for $V = +1.0$ V. The dominant peaks of the three Mo atoms have a strong component of non-directional *d* orbitals, resulting in a strong current contribution over the vacancy (instead of over the main Mo atoms), which corresponds to the large spot in the figure 6(c) image. On the other hand, when the bias is increased to +1.9 V, the S atoms start to contribute to the current, hence converting the spot into a depression, in good agreement with previous experimental observations [19, 22]. The same contrast change is observed for the filled state voltages, with a protrusion for low voltages and a depression for higher ones. Again, we can anticipate that the unbounded orbitals will probably be highly reactive to external adsorbates.

4.5. Sulfur antisite: one substitutional Mo atom

Starting from the previous configuration, we have now added a single Mo atom, substituting the removed S atom. This extra atom is placed 0.4 Å higher than the S atoms in the optimal structure superimposed in figure 7(a). As can be seen, this new Mo atom is now bonded to the three neighbouring Mo atoms and the two S atoms closest to the vacancy. This is reflected in the electronic DOS, shown in figure 6(b), by the emergence of several localised peaks attributed to the extra

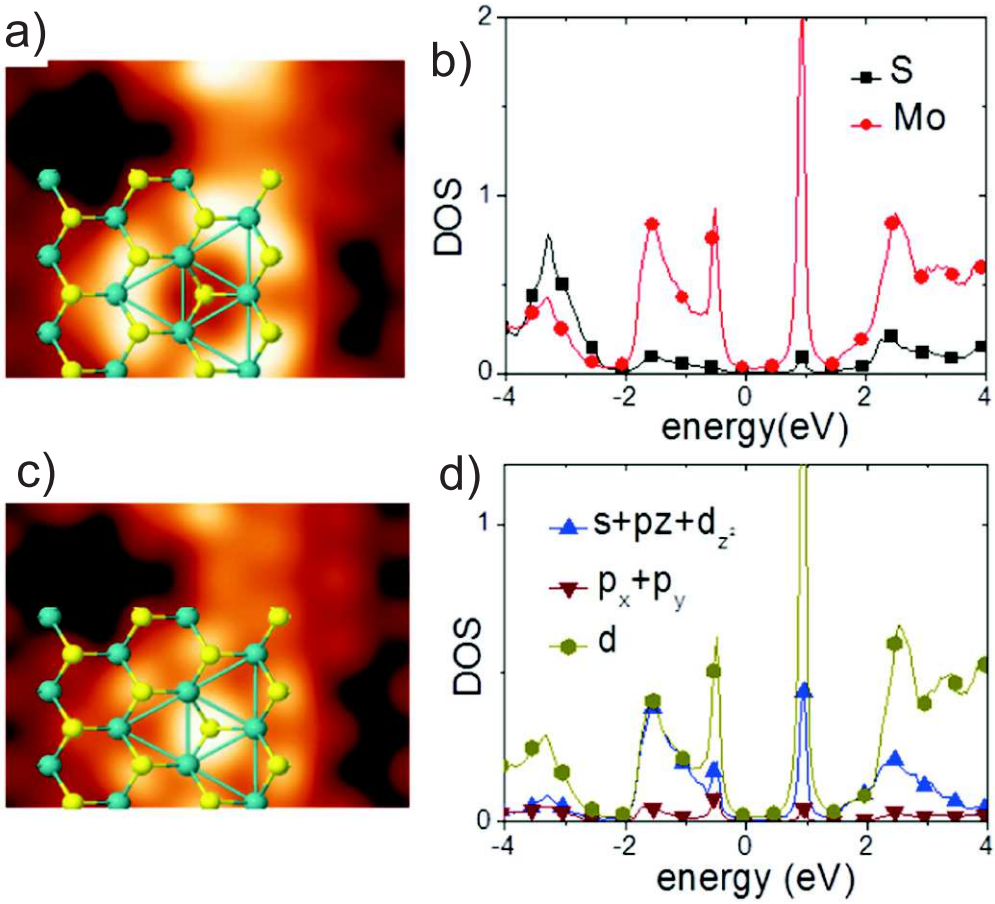

Figure 6. STM images of the corresponding unoccupied states, calculated at $V = +1.9$ V and $V = +1$ V, are represented in (a) and (c) for a sulfur vacancy in a MoS_2 monolayer. The atomic configuration is superimposed (yellow/blue spheres represent S/Mo atoms). The electronic DOS are represented in (b) for a S (black squares) and another Mo (red circles) atom around the vacancy and (d) shows the orbital contributions to the atomic DOS in the Mo atoms around the vacancy. The DOS are separated into directional $s + p_z + d_{z^2}$ orbitals (blue up-triangles), in-plane $p_x + p_y$ orbitals (red down-triangles) and the sum of the other four d orbitals (yellow hexagons).

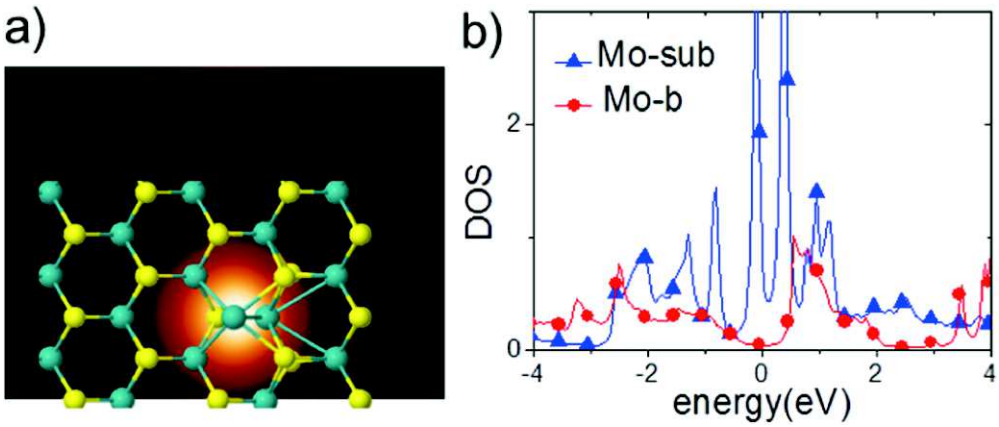

Figure 7. (a) STM image of the unoccupied states calculated at $V = +1.9$ V. The electronic DOS are represented in (b) for the Mo atom occupying the S vacancy (Mo-sub) (blue triangles) and a Mo atom bonded (Mo-b) with it (red circles). The new peaks come from the d orbitals (with an important contribution from the d_{z^2}.

Mo atom in the MoS_2 gap. These new states have a d-character, with an important contribution from the d_{z^2} orbital (not shown in the figure), which is responsible for the bright spot observed in figure 7(a). Here again, the DOS of the S atoms (not shown in the DOS figure) is not really affected. Due to the higher position of the substitutional Mo atom and its strong contribution to the DOS, the STM image does not change with the voltage, exhibiting the same behaviour in all the studied biases, namely a strongly localised spot over the extra Mo (or vacancy) site. Consequently, the removal or

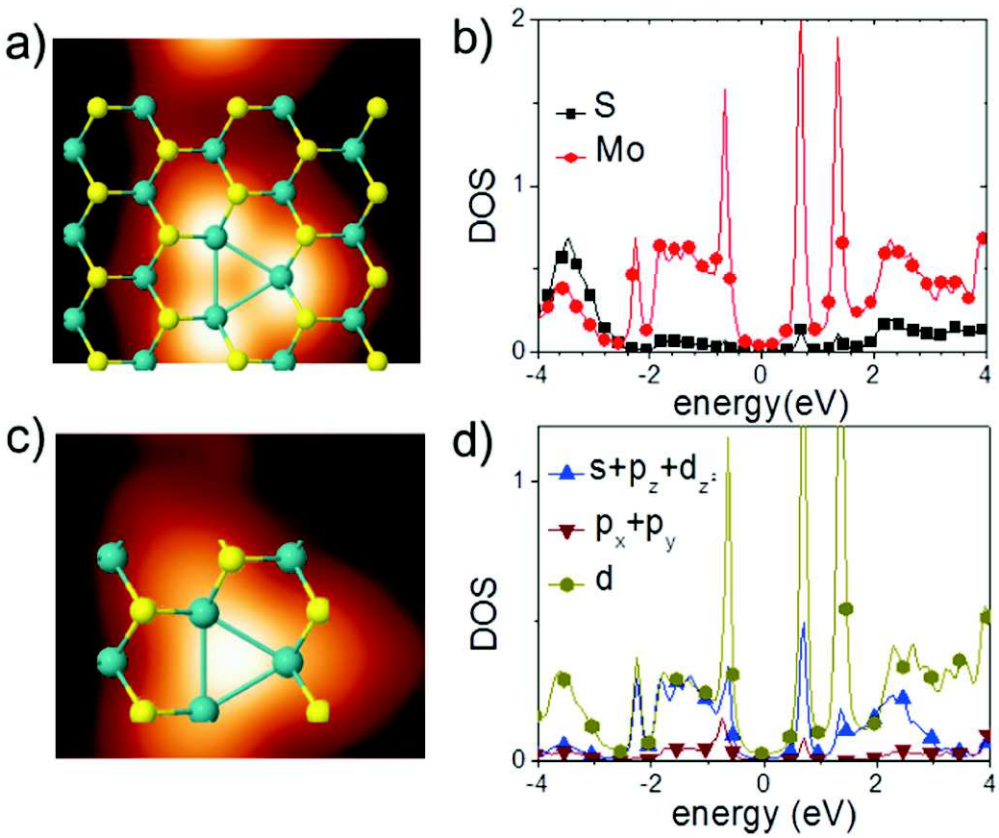

Figure 8. (a) Calculated STM image at $V = +1.9$ V for a 2S vacancy in a MoS_2 monolayer, with the corresponding atomic configuration superimposed (yellow/blue spheres represent S/Mo atoms), (b) the electronic DOS of a S (black squares) and a Mo (red circles) atom around the divacancy, (c) the STM image calculated at $V = -1.0$ V and (d) the orbital contributions to the atomic DOS in a Mo atom close to the vacancy. The contributions are separated into directional $s + p_z + d_{z^2}$ orbitals (blue up-triangles), in-plane $p_x + p_y$ orbitals (red down-triangles) and the sum of the other four d orbitals (yellow hexagons).

substitution of a S atom should also allow us to tune the reactivity of the site. The removal of one S atom creates a dangling bond that is 'shared' between the neighbouring Mo atoms, whereas its substitution by an Mo atom leads to the metallization of the system and the complete closure of the gap.

4.6. Sulfur divacancy

The last type of point defect considered is a divacancy formed by removing two S atoms initially bonded to the same Mo atom, i.e. both S atoms were originally placed at the same point in the *XY* plane, above and below the Mo layer (see the geometry superimposed on figure 8(a)). In this situation, the optimisation of the system has driven the Mo atoms close to the missing sulfurs to form new bonds between them, similar to the case of the single S vacancy. From an electronic point of view, the gap of the Mo atom has been reduced considerably to 0.8 eV, as seen in figure 8(b) and table 1, which is even smaller than for the single S vacancy case. Decomposing the DOS of the Mo atoms close to the divacancy, we obtain a similar result to that for a single S vacancy (see figure 8(d)), with a strong *d*-character for the new peaks (including some contribution from the directional d_{z^2}). On the other hand, no substantial changes can be seen for the S electronic density, except for the emergence of a very small density above the Fermi level, interpreted as being the creation of an unoccupied S state due to the charge rearrangement between Mo atoms. The DOS is also displayed in the calculated STM image for a voltage of +1.9 V (see figure 8(a)), where three brilliant traces localised on the reorganised Mo atoms can be clearly observed. They are closely related to the high value for the density of unoccupied states. By contrast, the image at +0.5 V and for filled states shows a single maximum over the vacancy (see figure 8(c)), exhibiting the different character of the orbitals dominating the different peaks in the DOS. The reduction of the gap points towards the higher reactivity of this site with the removal of the second S atom.

4.7. Sulfur divacancy antisite: one substitutional Mo atom

Starting from the divacancy structure, we can now add one Mo substitutional atom in the vacancy site. The corresponding optimised structure is represented in figure 9(a). The extra Mo atom (denoted Mo-sub) moves up 0.6 Å with respect to the Mo plane, still 0.9 Å below the upper S atoms. In this case, the Mo triangle disappears due to the bonds formed with the Mo-sub atom, but the corresponding excess of charges leads to a retraction of the surrounding Mo network. As a consequence, the emergence of many new Mo–

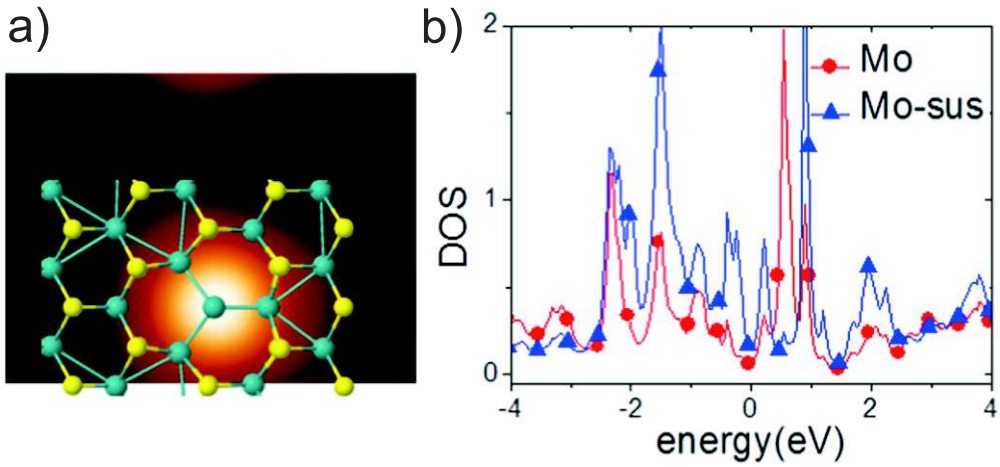

Figure 9. (a) Calculated STM image at $V = +1.9$ V for a 2S vacancy with a substitutional Mo atom (Mo-sub) in a MoS_2 monolayer. The atomic configuration is superimposed (yellow/blue spheres represent S/Mo atoms). The electronic DOS of a Mo atom close to the vacancy (red circles) and the Mo-sub atom (blue triangles) are shown in (b).

Mo bonds is observed in the monolayer. Of course, the electronic density is now greatly modified by the new substitutional atom, as displayed in figure 9(b). Hence, there is no gap in the Mo structure, as is to be expected because of the increased Mo proportion in the system. In that manner, the system tends to a purely Mo metallic network. Consequently, the MoS_2 layer is no longer electronically passivated and presents a pure metallic character, and therefore a much stronger reactivity. In addition, new peaks associated with the extra Mo atom emerge in the vicinity of the Fermi level, again presenting a strong *d*-character (not shown in the figure). In this case, the state at +1 eV has a d_{z^2} contribution, while the peak close to the Fermi level is formed by the sum of the other *d* orbitals. The interplay between the geometrical and electronic effects leads to a brilliant spot in the STM image for all the analysed bias (from −1.9 V to +1.9 V). It is important to note that this happens even though the substitutional Mo atom is 0.9 Å below the topmost S atoms, reflecting the great impact of the electronic effects in this case. The image at +1.9 V is presented in figure 9(a).

4.8. Sulfur divacancy antisite: two substitutional Mo atoms

Finally, the last structure we analyse contains two Mo atoms occupying the sites of the S divacancy. The final structure we obtain after the relaxation of the system presents a displacement of the new Mo atom of about 0.9 Å in the *X* direction, forming a kind of Mo row along the perpendicular *Y*- direction (see both directions in figure 1). This can be observed in the structure superimposed in figure 10(a). Again, the gap disappears. It is occupied by new peaks in the DOS related to the *d* orbitals (not shown in figure 10(b)) of the extra Mo atoms. As a result, the STM image now shows an even brighter spot that is explained by the geometrical and electronic arrangements. It is important to note that the current is more than 3.5 times larger over the new Mo atom here than in the previous case, under the same conditions of bias and tip–sample distance. This means that both defects can be distinguished easily in an experimental measurement. This important modification to the electronic conduction could also be exploited in new Mo–MoS_2 based nanoelectronic devices. The STM image for a voltage of +1.9 V is shown in figure 10(a), but the argument remains the same for all the biases (including empty and filled states).

As a conclusion inferred from studying the sulfur divacancy, we find that removing a second sulfur atom leads to a more reactive site than the previous single vacancy. Now, the inclusion of extra Mo atoms induces a more metallic behaviour than the opposite case where sulfur atoms are added to the Mo vacancy, inducing localised states in the gap of the semiconducting MoS_2 monolayer.

5. Conclusions

In conclusion, we have analysed by means of DFT simulations the atomic structure and electronic properties of the most prominent types of point defects in MoS_2 monolayers, namely atomic vacancies (where one S or Mo atom is removed), two sulfur vacancy (where two S atoms are removed) and the corresponding antisite cases. Our results confirm that geometry effects dominate in the STM imaging of S atoms for the pristine monolayer. When defects are present, a more complex situation is found and the STM images have a strong dependence on the applied bias in the cases of the pure vacancies and Mo antisites. The vacancies are imaged as large protrusions or dark holes, depending on the applied voltage, as also happens in the case of S atoms placed in the Mo vacancy. By contrast, when one or two Mo atoms occupy an empty sulfur site, a bright protrusion is obtained in the STM image, independently of the applied bias. Our electronic analysis suggests a strong reactivity for the defects as well as a potential modulation of the metallicity of the MoS_2 monolayer, paving the way to the study of the adsorption of different atoms or molecules that might tune and improve its

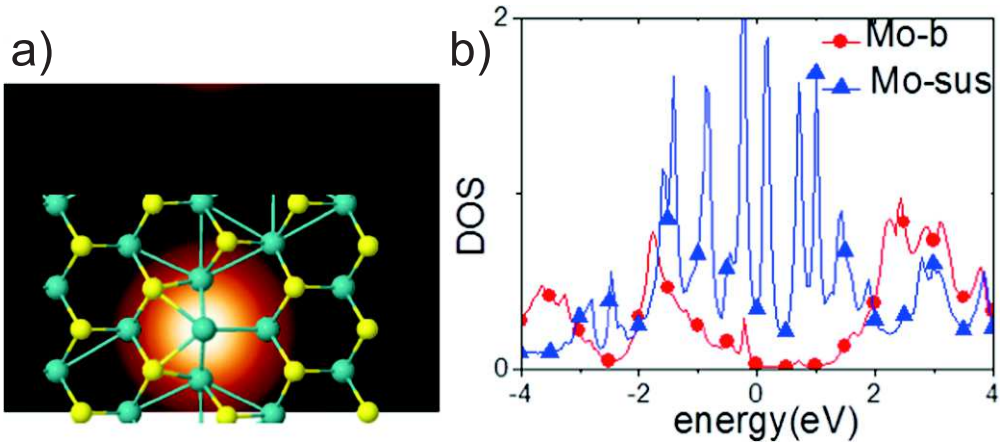

Figure 10. (a) Calculated STM image at $V = +1.9$ V for a 2S vacancy with two substitutional Mo atoms (Mo-sub) in a MoS_2 monolayer. The atomic configuration is superimposed (yellow/blue spheres represent S/Mo atoms). The electronic DOS of a Mo atom close to the vacancy (red circles) and the Mo-sub atom (blue triangles) are shown in (b).

capabilities for future nanoelectronics or gas sensor applications.

Acknowledgments

The authors acknowledge use of the computer resources of the Santander Supercomputacion group at the University of Cantabria, who provided access to the Altamira Supercomputer at the Institute of Physics of Cantabria (IFCA-CSIC), a member of the Spanish Supercomputing Network (RES) (project FI-2015–2-0004), and the Alhambra supercomputing facilities of the University of Granada. CG acknowledges funding from the Junta de Andalucía and the European Commission under co-funding from the 7th Framework Program in the People Program through the Andalucia Talent Hub program. BB's research is supported by MINECO (Spain) under the Ramon y Cajal program.

References

[1] Novoselov K S *et al* 2004 *Science* **306** 666
[2] Xu K, Cao P and Heath J R 2009 *Nano Lett.* **9** 4446
[3] Voloshina E N, Dedkov Y S, Torbrügge S, Thissen A and Fonin M 2012 *Appl. Phys. Lett.* **100** 241606
[4] Castro Neto A H, Guinea F, Peres N M R, Novoselov K S and Geim A K 2009 *Rev. Mod. Phys.* **81** 109
[5] Watanabe K, Taniguchi T and Kanda H 2004 *Nat. Mat.* **3** 404
[6] Dreyer D R, Park S, Bielawski C W and Ruoff R S 2010 *Chem. Soc. Rev.* **39** 228
[7] Kumar A and Ahluwalia P K 2012 *Eur. Phys. J.* B **85** 186
[8] Mak K F, Lee C, Hone J, Shan J and Heinz T F 2010 *Phys. Rev. Lett.* **105** 136805
[9] Jones A M *et al* 2013 *Nat. Nanotechnology* **8** 634
[10] Zhang Y *et al* 2014 *Nat. Nanotechnology* **9** 111
[11] Sørensen S G, Füchtbauer H G, Tuxen A K, Walton A S and Lauritsen J V 2014 *ACS Nano* **8** 6788
[12] Radisavljevic B *et al* 2011 *Nat. Nanotechnology* **6** 147
[13] Myoung N *et al* 2013 *ACS Nano* **7** 7021
[14] Thamankar R, Yap T L, Goh K E J, Troadec C and Joachim C 2013 *Appl. Phys. Lett.* **103** 083106
[15] Zhao S, Xue J and Kang W 2014 *Chem. Phys. Lett.* **595-596** 35
[16] Noh J-Y, Kim H and Kim Y S 2014 *Phys. Rev.* B **89** 205417
[17] Zhou W *et al* 2013 *Nano Lett.* **13** 2615
[18] Hong J *et al* 2015 *Nat. Comm.* **6** 6293
[19] Santosh K C, Longo R C, Addou R, Wallace R M and Cho K 2014 *Nanotechnology* **25** 375703
[20] Kodama N, Hasegawa T, Okawa Y, Tsuruoka T, Joachim C and Aono M 2010 *Jpn. J. Appl. Phys.* **49** 08LB01
[21] Lu C-P, Li G, Mao J, Wang L-M and Andrei E Y 2014 *Nano Lett.* **14** 4628
[22] Addou R, Colombo L and Wallace R M 2015 *Appl. Mat. Interf.* **7** 11921
[23] Voloshina E N, Fertitta E, Garhofer A, Mittendorfer F, Fonin M, Thissen A and Dedkov Y S 2013 *Sci. Rep.* **3** 1072
[24] Chen C J 1990 *Phys. Rev. Lett.* **65** 448
[25] Mann J *et al* 2013 *Eur. Phys. J.* B **86** 226
[26] Lauritsen J V *et al* 2007 *J. Catal.* **249** 220
[27] Lewis J P *et al* 2011 *Phys. Status Solidi* B **248** 1989
[28] Jelínek P, Wang H, Lewis J P, Sankey O F and Ortega J 2005 *Phys. Rev.* B **71** 2351011–9
[29] Sankey O F and Niklewski D J 1989 *Phys. Rev.* B **40** 3979
[30] Harris J 1985 *Phys. Rev.* B **31** 1770–9
[31] Foulkes W M C and Haydock R 1989 *Phys. Rev.* B **39** 12520–36
[32] Basanta M A, Dappe Y J, Jelinek P and Ortega J 2007 *Comput. Mater. Sci.* **39** 759
[33] Wakabayashi N, Smith H G and Nicklow R M 1975 *Phys. Rev.* B **12** 659
[34] Dolui K, Rungger I, Pemmaraju C D and Sanvito S 2013 *Phys. Rev.* B **88** 075420
[35] Han S W *et al* 2011 *Phys. Rev.* B **84** 045409
[36] Pu J, Yomogida Y, Liu K-K, Li L-J, Iwasa Y and Takenobu T 2012 *Nano Lett.* **12** 4013
[37] Huang Y L *et al* 2015 *Nat. Commun.* **6** 6298
[38] Mingo N *et al* 1996 *Phys. Rev.* B **54** 2225
[39] Blanco J M *et al* 2004 *Phys. Rev.* B **70** 085405
[40] Blanco J M, Flores F and Pérez R 2006 *Prog. Surf. Sci.* **81** 403
[41] Martínez J I, Abad E, González C, Flores F and Ortega J 2012 *Phys. Rev. Lett.* **108** 246102
[42] González C, Abad E, Dappe Y J and Cuevas J 2016 *Nanotechnology* **27** 105201
[43] Altibelli A, Joachim C and Sautet P 1996 *Surf. Sci.* **367** 209
[44] Horcas I, Fernández R, Gómez-Rodríguez J M, Colchero J, Gómez-Herrero J and Baró A M 2007 *Rev. Sci. Instrum.* **78** 013705 WSxM solutions www.wsxmsolutions.com